UM NM 72-1

Imaging in Nuclear Medicine with Incoherent Holography

W.L. Rogers, Ph.D.†, L.W. Jones, Ph.D.‡, and W.H. Beierwaltes, M.D.†
University of Michigan
November 1972

Text of invited talk delivered at Society of Photo-Optical Instrumentation Engineers Seminar on Application of Optical Instrumentation in Medicine. November 29,30, 1972, Chicago, Illinois.

† Department of Internal Medicine (Nuclear Medicine Division)

‡ Department of Physics

ACKNOWLEDGMENTS

The authors wish to acknowledge many helpful discussions with Jerry Shapiro, Emmett Leith, Adam Kosma, and Ki Han.

This work was supported by the National Institute of Health Grant GM 16188-03 and the Nuclear Medicine Research Fund.

INTRODUCTION

The problem of radioisotope imaging in nuclear medicine is to develop an image containing a maximum of information formed by γ-rays which in turn have been "focussed" by only aperture limitation. Gamma-emitting radiolabeled medicinals are designed to be concentrated by certain tissues. Abnormal regions may be indicated by either enhanced or reduced concentration of the labeled compound. The distribution of the radionuclides, as revealed by their γ-rays (e.g., 140 KeV in the case of ^{99m}Tc), may then be the basis for diagnosis not possible with X-rays or other nonsurgical techniques. Because the radiation exposure of the patient must be minimized, the images formed are limited by quantum statistics, and indeed the practical detectors are those which respond to single γ-ray quanta. The image quality available with current techniques is modest by the usual standards of X-ray or light imaging; a 25 cm diameter image field seldom contains more than 1000 resolved image elements. Indeed the total information content is often carried by a total of only 100,000 photons. Examples of isotope images useful for diagnosis are given in Figure 1: (a) a brain containing a tumor, (b) a frame of a cerebral blood flow study, and (c) a pair of adrenal glands. In view of the unique nature of the information gained, even this very modest image quality is invaluable in diagnosis. An illustration of this value is the fact that about 2,000,000 radionuclide diagnoses are now undertaken each year in the U.S.

UNIQUE ASPECTS OF THE NUCLEAR MEDICINE IMAGING PROBLEM

The essential problems in nuclear medicine imaging stem from the limited photon statistics available and from the penetrating nature of the radiation. These two aspects are closely related. The amount of information available is limited by four factors:

1) Maximum permissible radiation dose to the patient together with the fraction of the administered radioactivity which localizes in the region of clinical interest.
2) The length of time available for the study in terms of patient comfort and motion, cost, or (in the case of a dynamic function study) the duration of the event.
3) The inherent low efficiency of restrictive aperture imaging as fixed by the spatial resolution required for diagnosis.
4) The efficiency of the detector.

Items 3 and 4 relate directly to instrument design. The closest parallel problems in visible-light optics are those of night vision and astronomy where the statistics of single photons limit the image quality. As in the night vision problem, noise (dark-field signals) degrades the image, but unlike the night-vision problem, the γ-ray resolution is limited by the image-forming system as well as by photon statistics.

The lack of an image-forming system for γ-rays is a severe constraint. For practical purposes, there is no refraction or

reflection of γ-rays of energies of interest here (25 Kev-500 KeV). They are either transmitted or absorbed, or they undergo Compton scattering. One consequence of absorption is the reradiation of X-rays characteristic of the absorbing element; this together with the energy-degraded γ-rays from Compton scattering constitute serious sources of background.

The image-forming devices currently in use, therefore, are all various forms of opaque shields with small apertures. They fall into three classes: the pinhole, the multiple hole parallel channel collimator, and the multiple hole focussed collimator, as discussed below.

The detector design is influenced by these same factors. The detector must be constructed of dense, high atomic number materials in order to absorb the γ-ray with high probability, and it must convert this energy proportionally and efficiently to a detectable signal such that the spatial coordinates of the interaction are known. Proportional energy conversion is required because the Compton scattered γ-rays emanating from the patient have reduced energy and it is possible to reject most of these photons from the image by imposing an energy threshold.

CURRENT IMAGING TECHNIQUES

Historically, nuclear medicine is descended from the primitive surface scan of a patient by a diagnostician with a hand-held geiger counter, somewhat in the manner of a uranium prospector. The most widely-used technique in nuclear medicine, the scanner with a multi-hole focussed collimator, is the direct de-

scendant of this. The scanner typically consists of a sodium iodide crystal 3 or 5 inches in diameter coupled to a photomultiplier and mounted in a lead shield. The γ-rays enter through a collimator consisting of tapered holes which converge on a point in object space as illustrated in Figure 2b. The resolution can be expressed in terms of the radius of a circle of confusion, ρ, in the focal plane. In terms of the parameters on the figure, $\rho = a\frac{(A+B)}{B}$. The solid angle is given by $\Omega \propto \left(\frac{C}{2}\right)^2\left(\frac{a}{a+\epsilon}\right)^2$ *. The solid angle and resolution of course vary as functions of the object distance from the collimator. An image is obtained by translating the detector-collimator assembly along a rectangular raster and recording coordinates together with instantaneous counting rates. While the solid angle subtended by a scanner from each object point is relatively large, the image must be constructed from a time-sequential scan and the overall efficiency is relatively poor. The energy resolution of the scintillating crystal-photomultiplier combination is capable of rejecting most background γ-rays and X-rays.

A second class of detectors, on the other hand, may properly be called cameras as they integrate an entire image field simultaneously, albeit with a small solid angle subtended from each

*The expressions for resolution and solid angle here and below are approximate and illustrate the functional dependence on geometric parameters. The small-angle approximation is made and the effects of such details as collimator channel shape are ignored.

object point. Each of these cameras employs an image-forming aperture system and an imaging detector. The two common aperture systems are the pinhole and the parallel-channel collimator. The pinhole is the exact analogue of the optical pinhole, and the tradeoff between resolution and aperture is very obvious. In the example sketched in Figure 2a, $\Omega \propto \left(\frac{a}{2A}\right)^2$, the magnification m = B/A, and the circle of confusion in object space has a radius $\rho = \frac{a(A+B)}{2B}$. The parallel hole collimator, as illustrated in Figure 2c, has unity magnification, $\Omega \propto \left[\frac{a^2}{B(a+\epsilon)}\right]^2$ and $\rho = \frac{a(A+B)}{B}$. The collimator channels are typically round, square, or hexagonal. The septa thickness, ϵ, is matched to the γ-energy. In practice, the compromise between resolution and efficiency for these apertures has been arrived at empirically. Table I lists these parameters for some widely used commercial apertures.

Table I
Resolution and Efficiency for Three
Commercial Camera Apertures

Aperture	Geometric Efficiency	Theoretical Resolution at 10 cm.
4,000 Hole Tc^{99m} Parallel Hole Collimator, 25 cm. Field Diameter	1.44×10^{-4}	11 mm FWHM
16,000 Hole Tc^{99m} High Resolution Parallel Hole Collimator, 25 cm. Field Diameter	8.6×10^{-5}	8 mm FWHM
4.9 mm Diameter Pinhole	1.5×10^{-4}	7.4 mm

The image-forming detector could in principle be merely a sheet of X-ray film; however, the sensitivity of such films, even with the best intensifying screens, is far too poor to be of interest in nuclear medicine. The detector should be sensitive to single quanta and should image a substantial fraction of those reaching it to be useful. The most commonly used system, the Anger camera, uses a large slab (e.g., 11 in. diameter, 1/2 in. thick) of NaI(Tl) coupled to a matrix of many (19) photomultipliers. The summed signals provide the energy resolution, and the ratio between the various coincident pulse heights determines the x-y coordinate of the γ interaction. This method is capable of 8 mm resolution in the crystal independent of the image-forming aperture. As in the scanner, the detection efficiency of γ-rays reaching the crystal is high, ranging from 75% photopeak efficiency for the 122 KeV γ-rays from ^{57}Co to 11% for the 511 KeV γ-rays from ^{68}Ga.

THE ZONE PLATE APERTURE

Introduction

An alternative method of image formation in cases where refractive or reflective optics are not applicable was suggested by Mertz and Young in 1961 (Ref.1). They proposed the use of an aperture having the form of a Fresnel zone plate for the purpose of imaging X-ray stars. More recently, Barrett has suggested the application to nuclear medicine (Ref.2). The zone plates are of large scale so that diffraction effects related to the finite wavelengths of the X-rays are totally negligible. The

sources to be imaged cast shadows of the zone plate on the detector as shown in Figure 3. It should be noted that the angular position of the source is encoded by the coordinate of the shadow centroid, and that the distance of the source plane is encoded by the shadow diameter. Because the zone plate pattern is nearly identical to the hologram of a point source formed with coherent light, the shadow pattern obtained is referred to as an incoherent hologram. The shadow pattern is equivalent to an incoherent summation of point source holograms with the exception that it has a sharp spatial frequency cut-off resulting from the finite zone plate aperture.

In order to obtain an image of the original source distribution, a reduced scale transparency of the incoherent hologram is constructed and coherent (laser) light is projected through it. The zone plate image behaves as a lens for coherent light with focal length f given by

$$f = \pm \frac{R_1''^2}{\lambda}, \qquad (1)$$

where R_1'' is the radius of the image of the central zone in the scale of the transparency, and λ is the wavelength of the coherent light. Each image point is reconstructed at the focal point of its corresponding zone plate pattern. The method of reconstruction is shown in Figure 4. In the illustrated configuration the spatial frequency transform of the transparency is formed at the focal point of the incident converging beam. As with coherent holograms, two images are formed corresponding to the positive and negative focal lengths of the reduced zone

plate shadow pattern. If the magnitude of this focal length is greater than the transparency-to-transform-plane distance, d_p, both images will be brought to a real focus as shown. The illustration is for the case of an on-axis zone plate. In this situation the undiffracted beam and defocussed second image form a background which may be much more intense than the desired image. The undiffracted beam is brought to a sharp focus in the transform plane where it may be blocked by a stop as indicated. This leaves a background due to the defocussed second image. This problem may be avoided by using an off-axis aperture on the zone plate which excludes the center of the zone plate (Figure 5). The undiffracted beam continues along the optical axis defined by the center of the aperture. The real image is formed on the axis defined by the center of the zone plate, while the light corresponding to the second (often virtual) image is diffracted in the opposite sense such that it no longer contributes background to the real image.

It should be noted that the Fresnel zone plate aperture is not unique; other aperture configurations including a stochastic multiple pinhole array (as proposed by Dicke, Refs. 3,4) may be used to generate transforms in an analogous way. The virtue of the Fresnel zone plate is the relative ease with which the encoded image may be reconstructed.

The attractiveness of the zone plate aperture relative to a pinhole aperture lies in the increased solid angle efficiency offered by the zone plate for a given spatial resolution.

The object resolution for the on-axis zone plate is given (Refs. 1,5) as

$$\rho = \frac{A+B}{B} w, \tag{2}$$

where A and B are as shown in Figure 3 and w is the width of the smallest or outermost zone in the zone plate. Further,

$$w = (\sqrt{n} - \sqrt{n-1})\ R_1 , \tag{3}$$

where n is the number of zones and R_1 is the radius of the central zone. To obtain resolution equal to the on-axis zone plate in the same geometry a pinhole must have diameter w. The relative solid angle efficiency is given by

$$\eta = \frac{\Omega_{zp}}{\Omega_{ph}} = \frac{1}{2}\left(\frac{D_{zp}}{D_{ph}}\right)^2 . \tag{4}$$

For imaging simple point sources the zone plate diameter may be increased to fill the detector field at constant resolution by adding zones and increasing R_1 to maintain a fixed w. Solid angles orders of magnitude greater than for the pinhole may be attained. It should be noted that the expression for zone plate resolution must be modified in the case of an off-axis aperture on the zone plate. In this case the zone plate response must be convolved with the aperture response, and the spatial resolution of the zone plate is reduced by the ratio of the aperture radius, R_a, to the zone plate radius, R_p. In order to maintain object resolution, the zone plate scale must remain fixed and R_a must be increased to the original R_p by adding more zones. This results in increasing the detector resolution requirements by R_p/R_a. It should also be noted that the aperture must be circular to avoid an astigmatic response.

Signal to Noise for Infinite Counting Statistics

We have previously reported the imaging of simple gamma and optical sources (Refs. 6,7). Subsequently we have sought to separate the optical questions from the γ-ray problems, and in this section we report on results of optical analogue studies. The optical simulation forms a good analogue to the γ-ray application in the case of infinite counting statistics and sharp detector resolution. It offers the advantage of a much simpler experimental configuration and permits the use of film as a convenient and efficient detector. Here we examine the case of visible radiation and unlimited flux. Consider the geometry illustrated in Figure 3. The object consists of a collection of M point sources. Under the assumption that the transmission of the zone plate is cosinusoidal rather than binary and produces 100% modulation of a point source, the intensity distribution at the detector is given by:

$$I(x',y') = \frac{M\overline{I_o}}{2Z^2}\left[1 - \frac{1}{M\overline{I_o}} \sum_{i=1}^{M} I_{oi}\cos\left\{g(x'-h')^2 + g(y'-k')^2\right\}\right], \quad (5)$$

where

$$g = \frac{A^2\pi n}{Z^2 R_p^2}, \qquad h' = -\frac{B}{A}x_o, \text{ and } \quad k' = -\frac{B}{A}y_o .$$

The intensity of the i-th object point is I_{oi} and a sufficiently limited view angle is assumed so that the $\cos^3$ variation in intensity may be neglected. $\overline{I_o}$ is the average source intensity and Z is the source-to-detector distance. The radius of the zone plate is R_p and n is the number of zones.

The summation over the M object points must be terminated when the shadows no longer contribute to the point in question. This condition is given by

$$\left(\frac{A+B}{B} R_p - \frac{A}{B} x'\right) > x_o > -\left(\frac{A+B}{B} R_p + \frac{A}{B} x'\right) \tag{6}$$

with a similar expression applying to y_o. The first term in Equation (5) is a bias term which increases linearly with M. Since in practice the exposure of the hologram is controlled to maintain a fixed bias exposure, this dependence has been factored out of the expression. The second term is the modulation or information term which increases as $\sqrt{M}/2$ so that the fractional modulation in intensity of the shadow pattern decreases as $1/\sqrt{M}$.

Under the assumption that the hologram is recorded linearly, and that the film grain noise arises from film uniformly exposed to the bias level, the ratio of signal to film-grain noise in the reconstructed image may be calculated after the manner of Goodman and Kosma (Refs. 8,9,10) as

$$\frac{I_i(\alpha,\beta)}{\langle I_n(\alpha,\beta)\rangle} = \frac{\eta^2 K^2}{4M^2 \Phi_{\tau\tau'}(p_o, q_o)} \frac{(A_{si})^2}{A_t} \left(\frac{I_{oi}}{\overline{I_o}}\right)^2 . \tag{7}$$

In this expression $\eta = \chi M\overline{I_o}/(2Z^2)$ where χ is the slope of the amplitude transmittance versus exposure curve. Therefore η is the slope normalized to a fixed unit bias exposure. The spatial-frequency transmittance spectrum of the film grain noise, $\Phi_{\tau\tau'}$, has units of mm^2 per line. The areas A_{si} and A_t are the areas appropriate to the i-th signal and total hologram respectively, and K is a term depending on the film modulation transfer

function, MTF; K is nearly unity at the frequencies of interest to us. Also, $p_o = \alpha/(\lambda d_i)$ and $q_o = \beta/(\lambda d_i)$ define the central spatial frequencies appropriate to the point (α, β) in the image plane at distance d_i from the hologram.

Thus the signal-to-noise in incoherent holography varies inversely as the square of the number of object points, $1/M^2$, in contrast to $1/M$ as in coherent holography. It is also of interest to note from Equation (7) that intensity ratios in the image are squared relative to those in the object resulting in enhanced contrast. The presence of film grain noise as the only noise term implies that the second image and undiffracted beam have been eliminated by using an off-axis aperture on the zone plate.

It is instructive to examine the term containing the hologram areas for the case of shadow casting. A_{si} is the area of the hologram contributing to the i-th signal and in the on-axis case is just equal to the area of the minified zone plate shadow. It may be expressed in terms of the hologram focal length, f, the reconstructing wavelength, λ, and the number of zones, n, as

$$A_{si} = \pi n \lambda f \ . \tag{8}$$

Here only object points fully within the detector field of view are considered. A_t is just the detector field of view reduced to the scale of the hologram. This assumes that the area of the reconstructing beam is well matched to the information area of the hologram. If F is the detector field diameter and A and B are the object and detector distances as before, then A_t is

given by:

$$A_t = \frac{\pi}{4} n\lambda f \left[\frac{AF}{(A+B) R_p} \right]^2 , \tag{9}$$

and

$$\frac{A_{si}^2}{A_t} = 4\pi n\lambda f \left[\frac{R_p (A+B)}{F \quad A} \right]^2 . \tag{10}$$

This expression may be generalized to include the case of the off-axis zone plate aperture;

$$\frac{A_{si}^2}{A_t} = 4\pi n\lambda f \left[\frac{R_a (A+B)}{F \quad A} \left(\frac{R_a}{R_p} \right) \right]^2 .$$

Here R_a is the radius of the off-axis circular aperture on the zone plate of radius R_p. The values of R_a together with R_p and n also determines the number of resolution elements in the object which contribute overlapping shadows in the hologram corresponding to the limit expressed in Equation (6).

If film grain noise is the dominant noise, an estimate of the object dynamic range and number of superimposed point source holograms which will result in an acceptable signal-to-noise in the reconstructed image may be calculated. Goodman has pointed out that the measure of signal-to-noise important in holography is the signal to standard deviation of the noise (Ref.8),

$$I_i/\sigma \cong \left[I_i / 2\langle I_n \rangle \right]^{1/2} . \tag{12}$$

It is instructive to consider the following numerical example:

R_p = 12 cm F = 25 cm

n = 60 zones f = 150 cm

R_a = 4 cm I_i/σ = 2

$$\frac{I_{io}}{I_o} = \frac{1}{5} \qquad \lambda = 6.3 \times 10^{-5} \text{ cm}$$

$$A = B .$$

The highest spatial frequency in the hologram, ν_{max}, is given by:

$$\nu_{max} = \frac{n}{\sqrt{n\lambda f}} = 8 \text{ lines/mm.}$$

Using film characteristics for Kodak 649-F from Ref. 9 gives:

$$\eta = 0.56 , \qquad \Phi_{\tau\tau'}(p,q) \cong 1 \times 10^{-10} \text{cm}^2/\text{line}$$

$$K \approx 1 .$$

Substituting these parameters into Equations (7), (11), and (12) yields a value for M_{max} of 550. That is, for the stated conditions, 550 sources may have overlapping shadows.

EXPERIMENTAL RESULTS WITH OPTICAL SOURCES

Our experiments with optical sources confirm the predicted trends, but we have not yet been able to reach the theoretical limits for the number of object points. Figure 6 illustrates the decrease in signal intensity as the number of object points is increased. The background which, in this case, includes both the second image and the undiffracted beam is held roughly constant.

It was implied in the signal-to-noise derivation that M is the number of resolved point sources. It is apparent that a large continuous source will rapidly cause the hologram modulation to disappear into the film grain noise. This problem has

been partially solved by spatially modulating the source with a half-tone screen of spatial frequency determined by the highest spatial frequency of the zone plate and the relative distances of the object, zone plate, and detector (Refs. 7,11).

The screen has two effects. It increases the modulation in the hologram and also permits use of an off-axis zone plate, which has no "DC" response, on continuous objects.* Figure 7 illustrates the effect of the half-tone screen on the image of the letters U o M. The letters were backlighted by a diffuse light source, and a half-tone screen with a spatial frequency of 0.5 cycles/mm was superimposed on the letters. A 40 zone, 62 mm diameter, on-axis emulsion zone plate was placed 15 cm from both the letters and a rear projection screen. The shadow pattern was photographed from the rear of the screen. The increase in signal-to-noise with the addition of the half-tone screen is evident.

In coherent holography the magnitude of the bias term is controlled by the amplitude of the reference beam. In incoherent holography the experimenter has no control of the bias which in this case is governed by the number of overlapping shadows. In practice, the bias varies slowly from a minimum at the edge of the hologram to a maximum toward the center. To record the entire pattern demands a film with a dynamic range M times the exposure required to exceed the fog level, where M is also the number of object points giving overlapping shadows. This implies a low contrast recording. The signal to noise in the reconstructed image, however, depends on χ^2 where χ is the slope of the trans-

*Similarly, for an on-axis zone plate, it permits blocking the undiffracted beam.

mittance versus exposure curve. We have employed photographic masking in an effort to solve this problem. The original shadow pattern is recorded on Polaroid type 55 P/N film. A blurred contact print is made of the negative and developed with a γ of 1. The exposure is regulated so that the maximum density of the mask is equal to the maximum density of the negative. When properly made, the average density of the mask plus negative is constant and only the higher spatial frequencies of the signal remain. The mask and negative are then superimposed and copied with the proper reduction in size on Agfa 10-E-75 film which is developed 5 minutes in D-19 to yield a high contrast fringe pattern. This masking process is illustrated in Figure 8. The object plus half-tone screen is shown in 8a, a high contrast copy of just the negative in 8b, and a high contrast copy of the negative plus mask in 8c. The reconstructed image made from 8c is shown in 8d. The object in this case contains about 230 resolved points. The masking and high contrast copying process yields increased signal and a more uniform image. The effect of the masking is most apparent in the added fringe stucture visible in Figure 8c over that in 8b. A more complex object containing 650 points and two intensity levels is shown in Figure 9a. The reconstruction from an on-axis hologram is shown in 9b and that from an off-axis hologram is shown in 9c. The overall quality leaves much to be desired, but one can discern the improved signal to noise for the off-axis case. Improved masking techniques should yield even better results. The on-axis holograms in Figure 8 and 9 were made with

a 22 zone, 2.3 cm diameter zone plate with A=B=20 cm. The off-axis hologram was made with a 40 zone, 3.1 cm diameter zone plate. The aperture radius, R_a, was 6 mm, and in this case the calculated value for M_{max} was 585 for $I/\sigma = 2$. It should be added that for this scale zone plate diffraction effects were minimal although still observable.

APPLICATION TO GAMMA RAYS

We have studied incoherent holography with visible radiation in order to gain some understanding of the techniques and an appreciation of the problems involved. In making the transition to γ-rays two additional problems assume a prominent position: the limited number of photons, and the difficulty of efficiently detecting these photons with good spatial resolution. It is hoped that the increased aperture available with the zone plate will help alleviate the first of them. However, use of the zone plate, and in particular the off-axis zone plate, creates a need for detector resolution which exceeds the capabilities of the Anger camera by a factor of three, even if no improvement in system resolution is sought. Furthermore, the Anger camera would be pressed to be able to handle some of the increased count rates encountered with a zone plate aperture.

The Michigan high resolution image intensifier camera has proven very successful in both of these respects (Refs. 12,13). Figure 10 illustrates the camera with a zone plate aperture. The γ-rays are detected in the 1/4 in. thick sodium iodide crystal with a diagonal of 11 in. The crystal is hexagonal, and is equipped with edge windows in addition to the glass

coverplate at the rear. The edge windows permit pulse height analysis and will not be discussed further here. The crystal is interchangeable with an X-ray intensifier screen or an optical test pattern. Some of the light leaving the rear of the crystal or screen is imaged through an f/0.87 objective lens onto the first-stage photocathode of the EMI 9692 image intensifier tube. The image intensifier is a 2 in. diameter, four stage, magnetically focussed tube which is capable of being gated. It has a luminous gain of 10^6 with extremely low noise; less than 200 electrons per cm^2-sec. The output phosphor is photographed with either Polaroid or 35 mm film. A photograph of the camera with zone plate is shown in Figure 11. This zone plate has an outer ring width of 1 mm and a solid angle efficiency 30,000 times that of a 1 mm pinhole, and yet it is capable of the same theoretical spatial resolution.

The camera has an intrinsic linespread function of 1.5 mm full width at half maximum for ^{57}Co as shown in Figure 12. Figure 12 also illustrates one of the difficulties encountered: the edge response for a 30% field flood has a long tail of about 7-8% of the peak intensity. This is caused by light scattered out of the crystal due largely to a poor surface finish. If a calcium tungstate X-ray intensifier screen is substituted for the crystal, and 80 KeV γ-rays from ^{133}Xe are used as a source in place of the 122 KeV cobalt γ-rays, the tail is dramatically reduced.

Figure 13 illustrates the resolution obtained with ^{133}Xe and

the X-ray screen. Image a) is the transmission pattern of a lead zone plate. The narrowest ring is 1 mm wide. Image b) is the transmission pattern of a lead half-tone screen. The holes are 3 mm diameter and spaced 5 mm center-to-center. The "S" distortion characteristic of magnetically focussed tubes is evident and has a peak amplitude of about 1 mm. The dark bar occupying the exact center of the image is the result of an accidental burn of the last stage photocathode. It is an interesting consequence of zone plate imaging which makes this burned area significantly less damaging to the reconstructed image than to a conventional image.

The intrinsic efficiency of this camera with the sodium iodide crystal is about 12% for 140 KeV γ-rays. This efficiency can be significantly increased by going to a large diameter photocathode, unconventional optics, a more efficient first cathode, or more efficient scintillator. The efficiency of the camera plus collimator, however, will be increased with a zone plate aperture. Just how much of the increased solid angle efficiency will be reflected as increased signal-to-noise in the image, and how the signal-to-noise will depend upon the number of source elements is presently under study. The controlling noise factor is expected to be the statistical fluctuation in the bias term arising from the finite number of γ-rays.

In Figure 14 we show a standard thyroid phantom, a 1 mm pinhole image of the phantom, and two reconstructed zone plate images. The phantom was loaded with 5 m Ci of ^{99m}Tc. This relatively high activity was used to eliminate tube noise as a

problem as the tube was not operated in the gated mode for these tests. The tube noise is nevertheless evident in the pinhole image, which was a 2 minute exposure. In this image (Figure 14b) the left lobe of the thyroid is barely visible because a 1 mm diameter pinhole in 1.5 mm lead severely vignettes the field off-axis. This image was recorded on Polaroid type 57 film. The zone plate image was made with an on-axis, 20 zone, 9 cm diameter zone plate made of 1 mm thick lead. A lead half-tone screen with 2.25 mm holes spaced 6 mm on centers was located 15 cm from the zone plate which in turn was spaced 10 cm from the detector. The source-aperture-detector spacing was the same for the pinhole. The hologram from which Figures 14c and 14d were reconstructed was recorded on the very slow Polaroid type 55 P/N film. A four minute exposure was required because of this slow film speed. Holograms of apparently equal quality could be recorded on type 57 Polaroid film in 30 seconds.

The images of Figures 14c and 14d were reconstucted from the same hologram in slightly different ways. In 14c, four apertures were placed in the spatial frequency plane to permit simultaneous recording of the positive and negative x and y orders corresponding to the object modulated by the half-tone screen. The effect of the screen is clearly visible. In 14d, however, the information on the four orders was recorded sequentially. While one would expect that only the positive or the negative orders would be necessary to reconstruct the image, because of the finite nature of the zone plate aperture there

remains a strong correlation between regions in the hologram and regions of the object. Since the fractional modulation in the center of the hologram is reduced by the increased bias at the center, different sides of the on-axis zone plate contribute varying amounts of information concerning different regions of the object. This has the effect of unevenly dividing the object information among the various diffraction orders. The photographic masking discussed earlier reduces this effect but does not entirely eliminate it.

Because of the near impossibility of subtracting the bias when film is used as a detector, and because of the dynamic range limitation imposed by film along with the extended processing time, we feel that it is important to consider digital processing as an alternative to optical processing. Certainly, the bias may be readily removed with minimal addition of noise. Dynamic range is no problem, and the number of resolution elements is modest compared to current image processing capabilities. One could conceive of a combined processor in which the computer is used to record the signal, remove the bias, and generate a hologram on a thermo plastic recording medium. The image might then be reconstructed optically with very minimal time delay.

It may also be possible to use the computer to make the real image without the intermediate step of an optical hologram. This might be done either in direct analogy to the optical reconstruction with coherent light, or (more simply) using the computer analogue of the incoherent optical reconstruction (Ref.3). It appears possible in this case to build a real-time image on

an output oscilloscope screen as the camera is integrating the holographic image data. This technique, however, appears to sacrifice signal-to-noise ratio relative to coherent reconstruction.

We have not yet quantitatively explored the relationship between photon statistics, camera and zone plate resolution, and number of resolved object (source) elements. Qualitatively it is clear that the required photon statistics for a given object complexity are greater than in the corresponding pinhole case, thus cancelling in part the gain in camera speed suggested by the simple solid angle factors.

CONCLUSIONS

We believe that the zone plate imaging system opens a new dimension in imaging techniques for nuclear medicine. This field is still in its infancy, and considerable research is still needed, both theoretically and experimentally. Nevertheless, the dramatic gain in solid angle apparent here should lead to valuable applications. In general, it appears that zone plate imaging would be more useful with small-area, faint sources (such as adrenals) than with diffuse, large sources containing possible voids (such as livers). The potentialities of the zone plate seem particularly well-matched to the higher-resolution, lower efficiency characteristics of the image intensifier camera. We look forward to the early perfection of a clinically-useful system based on these principles.

Figure Captions

Fig. 1. Examples of useful radionuclide images. (A) Rectilinear scan of brain with tumor. Scanning time was about 12 minutes and peak information density is 800 photons/cm^2. Focal plane resolution of the collimator is 1.2 cm F.W.H.M. (B) A two second frame of a cerebral blood flow containing about 7,000 photons made with an Anger camera using a low energy 4,000 hole parallel channel collimator. In both (A) and (B) 15 mCi of ^{99m}Tc pertechnetate was injected. (C) A ten minute image of a pair of diffusely overactive adrenals containing about 1,000 counts per adrenal. Image was made with Anger camera using medium energy, 1,000 hole parallel channel collimator.

Fig. 2. Types of apertures used in nuclear medicine imaging.

Fig. 3. Incoherent coding of a source distribution using a Fresnel zone plate aperture. The scale of the zone plate is chosen to make diffraction effects totally negligible and the geometric shadow pattern is recorded by the detector.

Fig. 4. Coherent decoding of the zone plate shadow pattern obtained with an on-axis zone plate. Reconstruction is performed in a converging beam. Image A corresponds to the positive focal length of the hologram while image B corresponds to the negative focal length.

Fig. 5. Illustration of an off-axis aperture on a zone plate. The remainder of the zone plate is shown only to clarify the dimensions.

Fig. 6. Illustration of the decrease in signal-to-noise in the reconstructed image as the number of object points is increased. The background is kept approximately constant.

Fig. 7. Effect of a half-tone screen on the reconstructed image. A 0.5 cycle per mm screen was superimposed over the backlighted, 3 cm high letters. A 40 zone, 62 mm dia., on-axis zone plate was used with A = B = 15 cm.

Fig. 8. Effect of masking to remove the variation in bias exposure. (A) A 230 point uniform object with a superimposed 1 cycle per mm half-tone screen. An on-axis zone plate was used with R_p = 1.15 cm and n = 22 zones. A = B = 20 cm. (B) A high contrast copy of the shadow pattern showing loss of information in the light and dark regions caused by variation of the bias exposure. (C) A high contrast copy of the masked shadow pattern showing an increased number of "fringes" and reduction of the bias variation. The remaining variation is the result of non-uniform development of the mask. (D) Reconstruction of the object from a high contrast copy of the masked negative. Note improved uniformity compared to Fig. 7. The residual non-uniformity results from the non-uniform mask and non-linearities in the original shadow pattern recording.

Fig. 9. (A) A 650 point object with two intensity levels shown with superimposed half-tone screen. The spatial frequency of the screen is 1 cycle per mm. (B) Reconstruction from an on-axis hologram. A = B = 20 cm, R_p = 1.15 cm, n = 22 zones. The primary background comes from the defocused second image. (C) Reconstruction from an off-axis hologram showing improved signal-to-noise. A = B = 20 cm. Rp = 1.55 cm, Ra = 6 mm, n = 40 zones.

Fig. 10. Diagram of the image intensifier radioisotope camera with Fresnel zone plate aperture. Light from the scintillations in the ¼ in. thick sodium iodide crystal is imaged through the f/0.87 objective lens onto the photocathode of the EMI 9692 image intensifier tube. The output is photographed directly with Polaroid or 35 mm film.

Fig. 11. The image intensifier camera with zone plate aperture.

Fig. 12. Edge response and intrinsic line spread function of the image intensifier camera for ^{57}Co. The long tail observed in the edge response to a 30% field flood is caused by light scattering in the crystal arising from a poor surface finish.

Fig. 13. Illustration of the intrinsic resolution of the image intensifier camera with ^{133}Xe and a calcium tungstate intensifier screen. The dark bar in the center of the images is the result of an accidental burn of the 4th stage photocathode. (A) Transmission pattern of a lead zone plate obtained with a distant point source. The narrowest ring is 1 mm wide. (B) Transmission pattern of a lead half-tone screen. The holes are 3 mm diameter and spaced 5 mm center-to-center. The "S" distortion characteristic of magnetically focused tubes has a peak amplitude of about 1 mm.

Fig. 14. (A) Photograph of Picker thyroid phantom. The right lobe contains an average activity of twice that of the left lobe. It also contains 2 "cold" nodules 5 mm and 12 mm diameter. The left lobe contains an 8.5 mm diameter "cold" nodule and a 12 mm diameter "hot" nodule. (B) Image of thyroid phantom taken with 1 mm pinhole and image intensifier camera. Phantom contained 5 mCi of ^{99m}Tc. A = 15 cm, B = 10 cm. Duration of exposure was 2 minutes using Polaroid type 57 film. The large cold nodule is visualized clearly. The left lobe is poorly visualized because the 1 mm diameter pinhole in 1.5 mm thick lead had a restricted view angle even though the pinhole edges are beveled. (C) Reconstruction of thyroid image made with a 1 mm thick on-axis lead zone plate and half-tone screen. Rp = 4.5 cm, n = 20 zones, w = 1 mm, A = 15 cm, B = 10 cm. The halftone screen had 2.25 mm holes spaced 6 mm center-to-center. The hologram was recorded with a 4 minute exposure on Polaroid type 55 P/N film. Holograms appearing equal in quality could be recorded in 30 seconds on type 57 film. The reconstruction was obtained by placing 4 apertures on the image spectra in the spatial frequency transform plane and recording the information in these spectra simultaneously. (D) This image was reconstructed from the same hologram as image C). The only difference is that the information coming through the 4 apertures was recorded sequentially. Both C) and D) differentiate the hot and cold lobes of the phantom and the hot nodule. The cold nodules are not visualized.

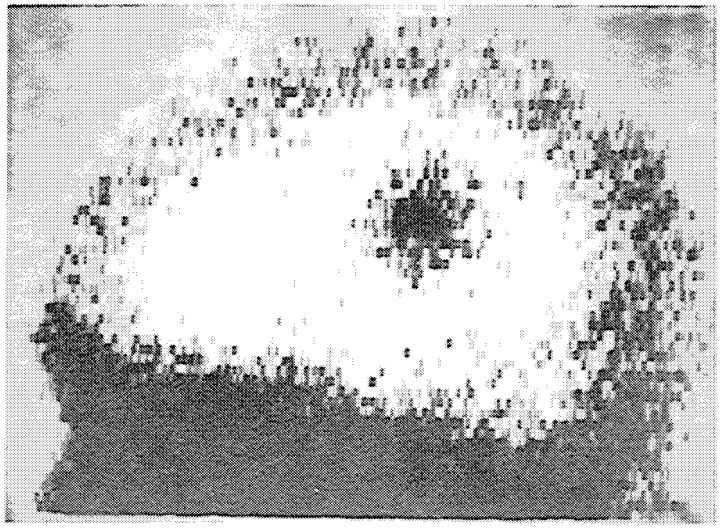

A

B

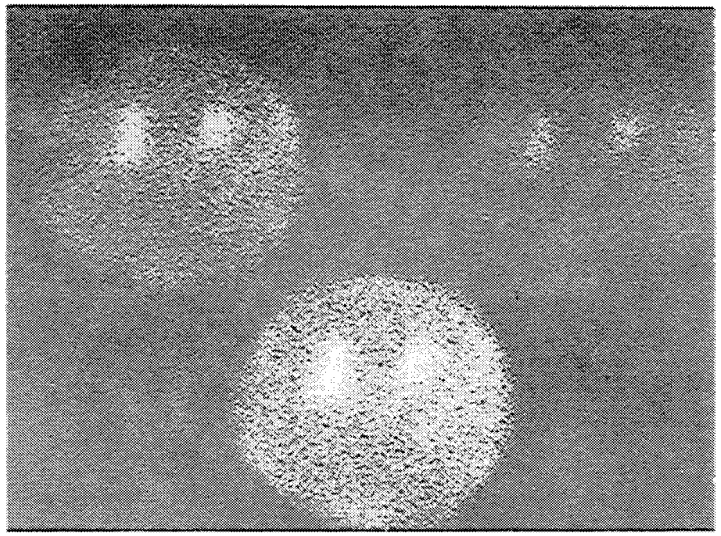

C

Figure 1.

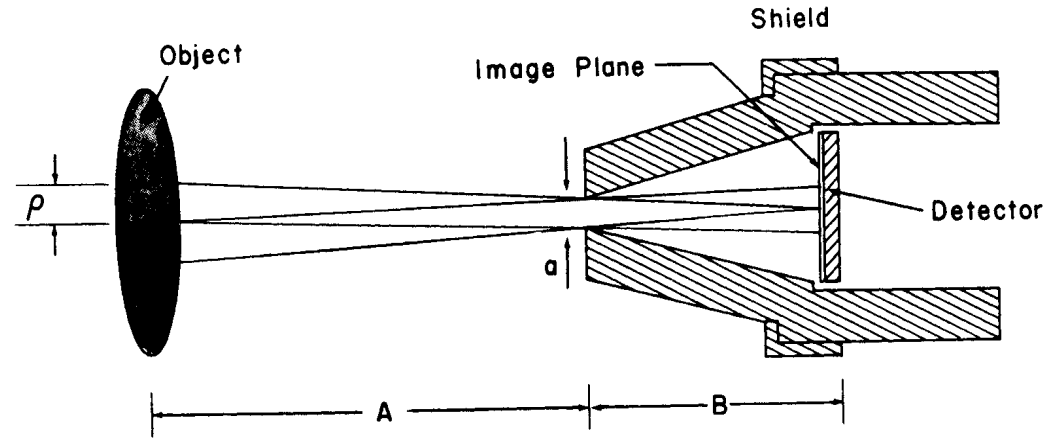

a

PINHOLE

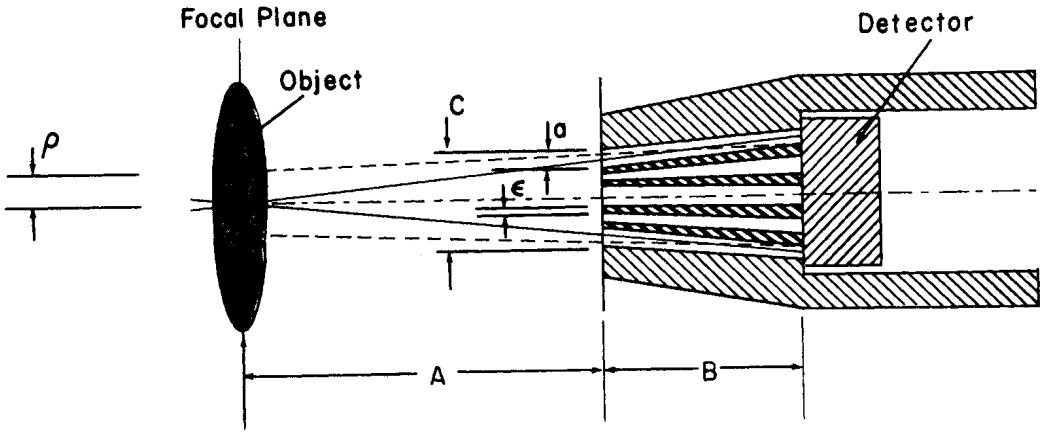

b

FOCUSED COLLIMATOR

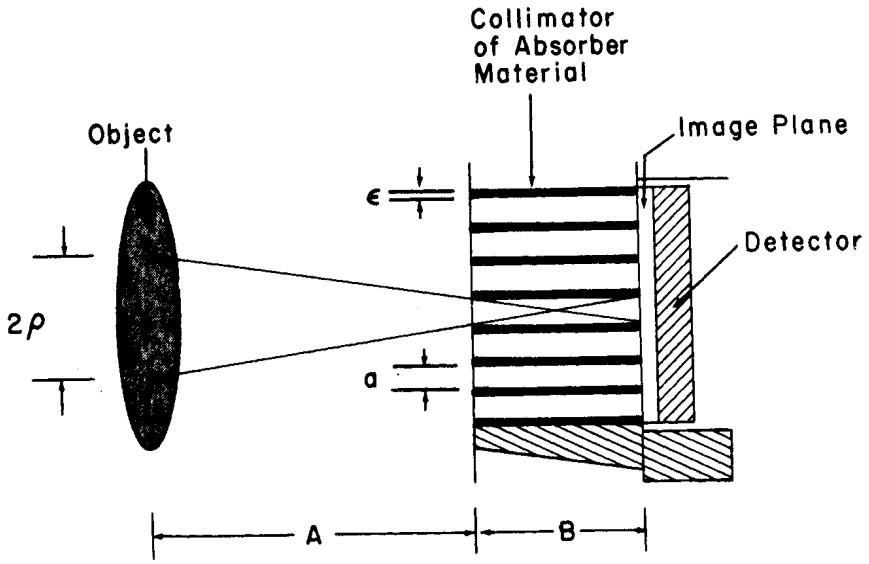

PARALLEL HOLE COLLIMATOR

Figure 2.

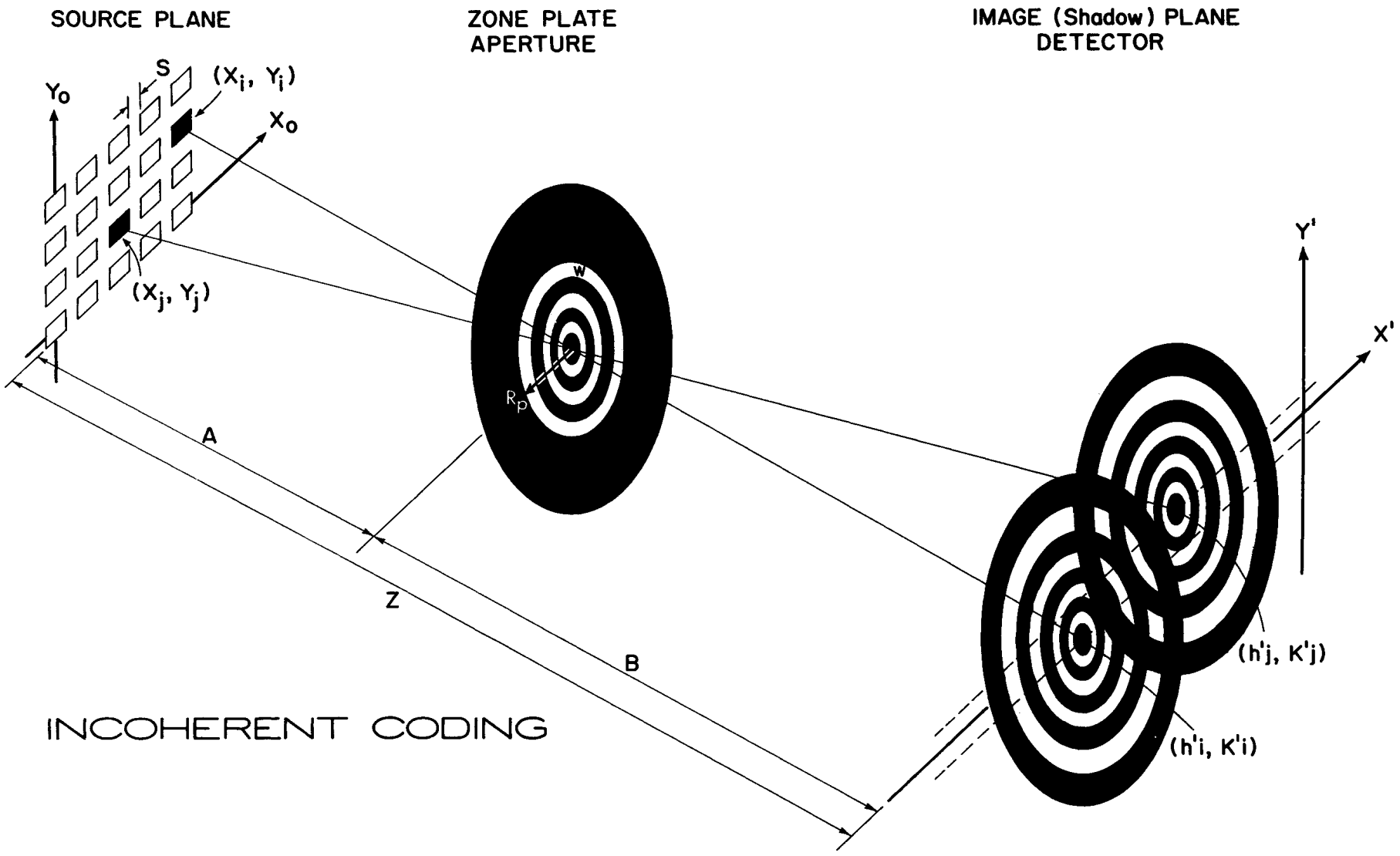
SOURCE PLANE
ZONE PLATE APERTURE
IMAGE (Shadow) PLANE DETECTOR
S
(X_i, Y_i)
Y_o
X_o
(X_j, Y_j)
w
R_p
A
Z
B
Y'
X'
(h'j, K'j)
(h'i, K'i)
INCOHERENT CODING

Figure 3.

COHERENT DECODING

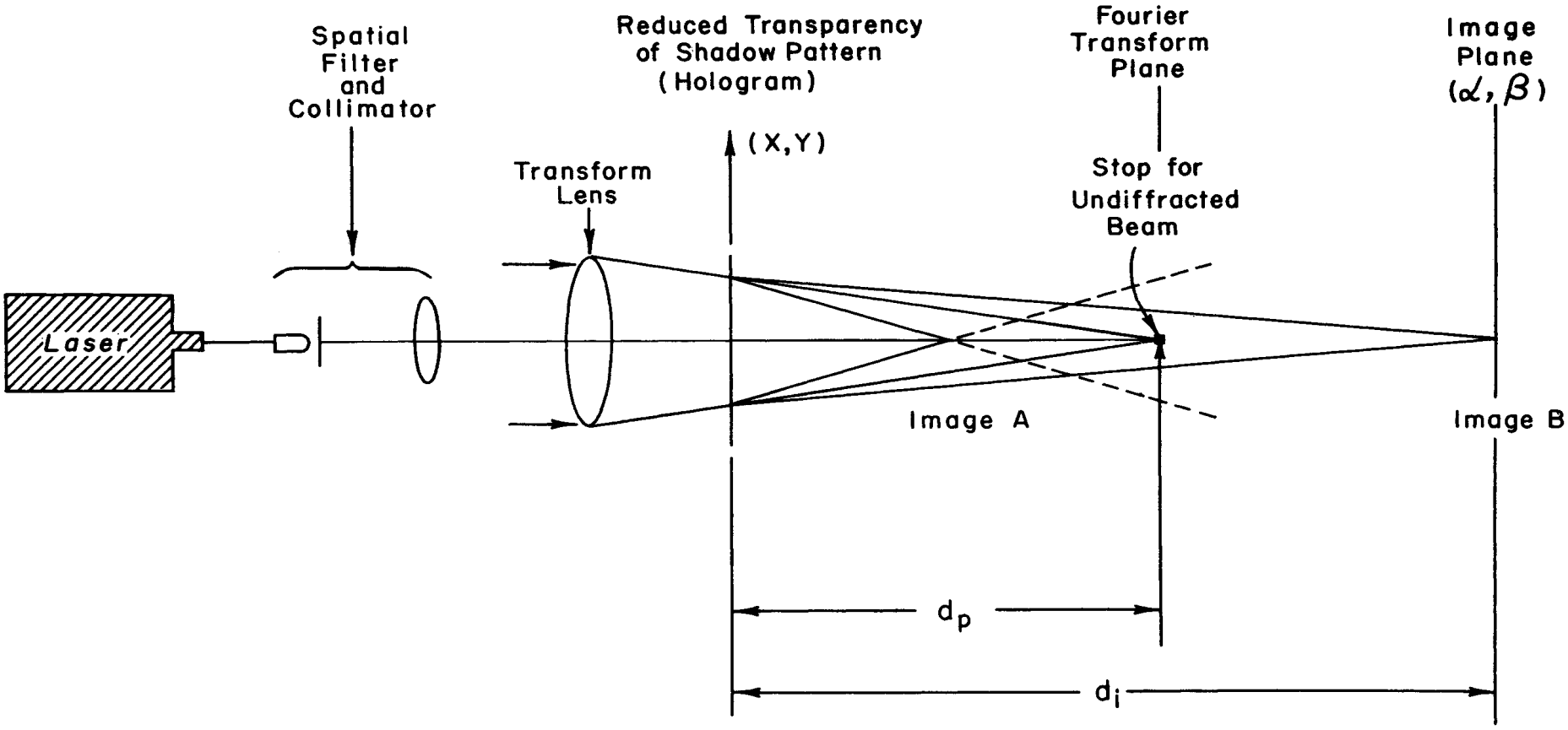

Figure 4.

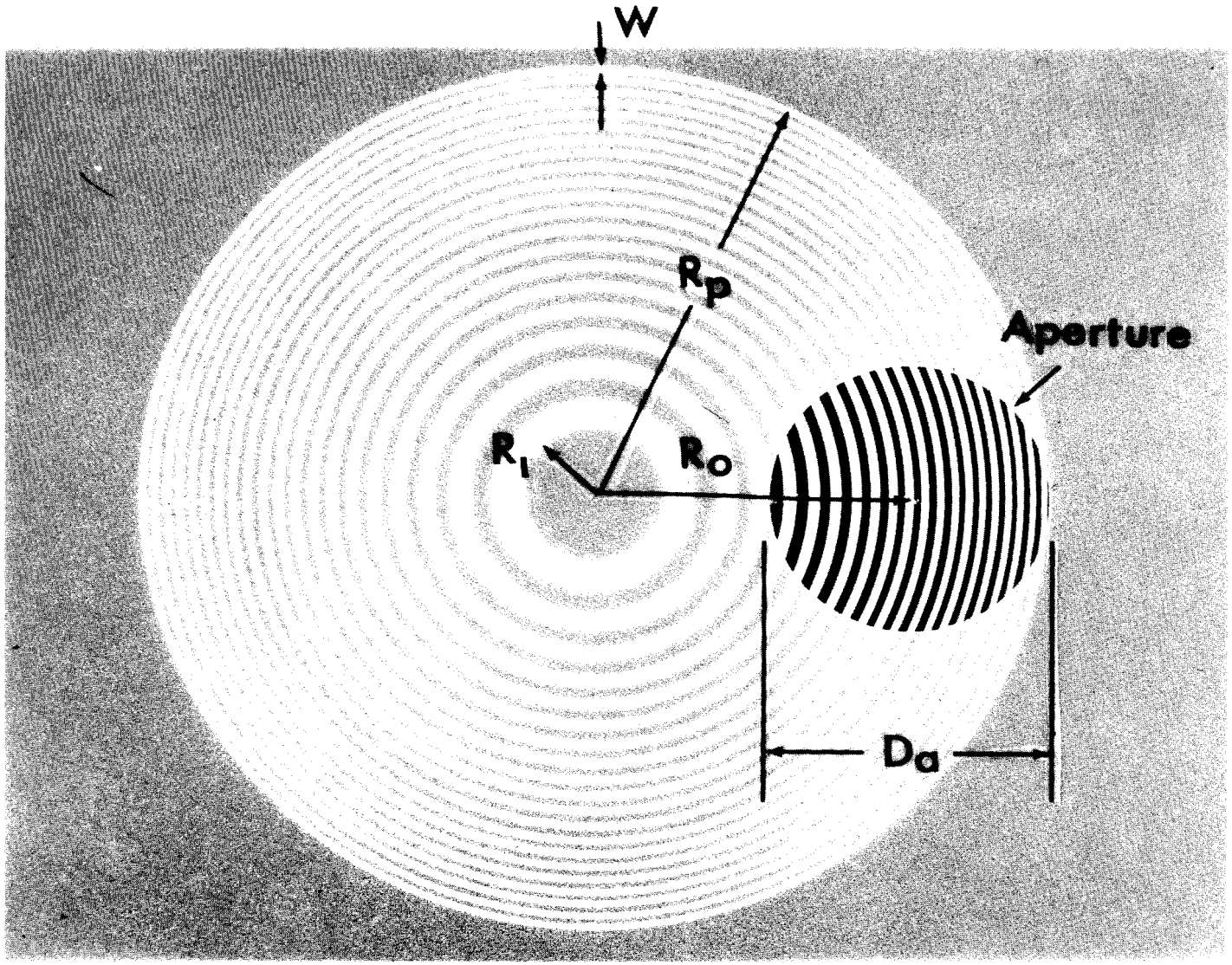

OFF AXIS APERTURE ON ZONE PLATE

Figure 5.

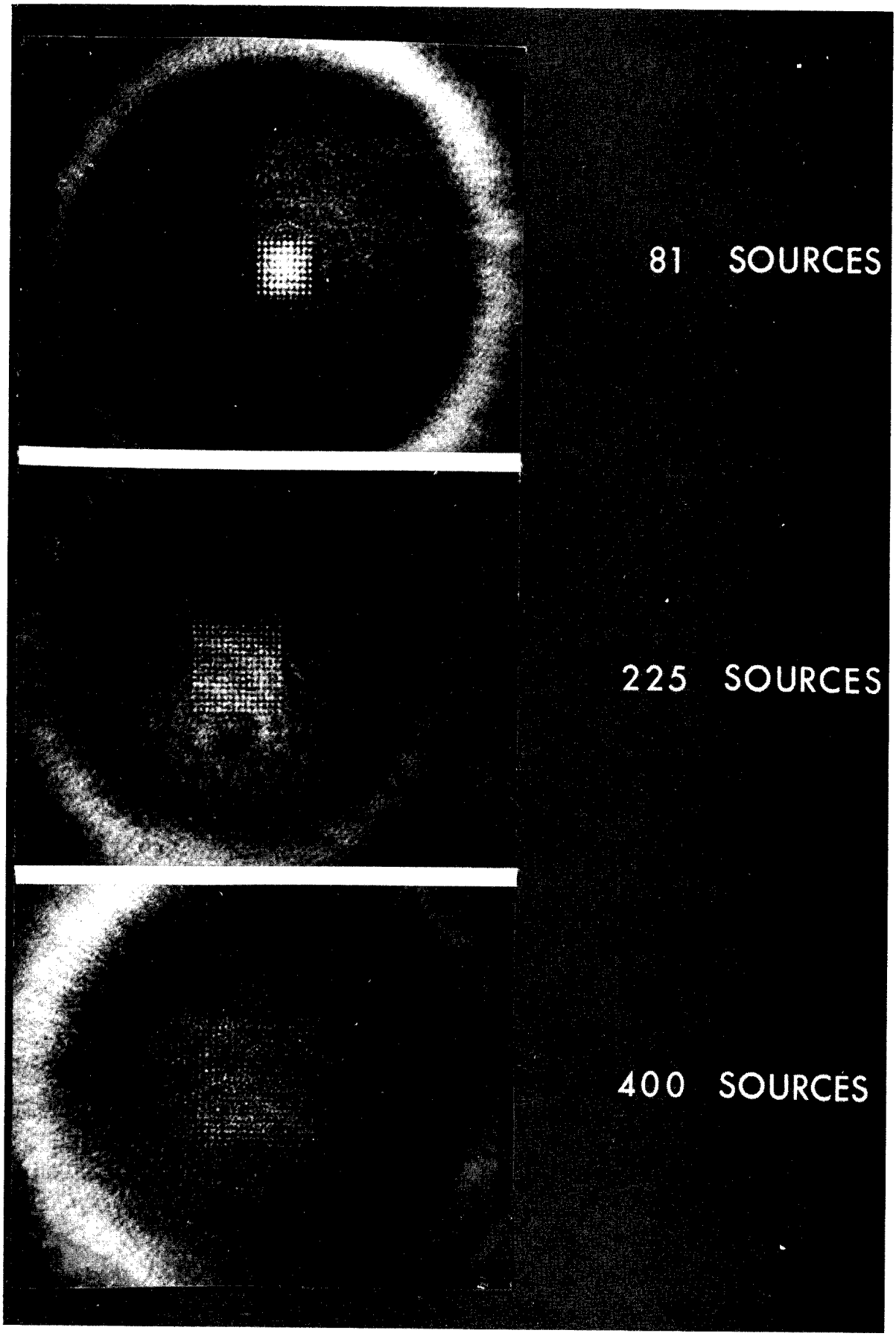

Figure 6.

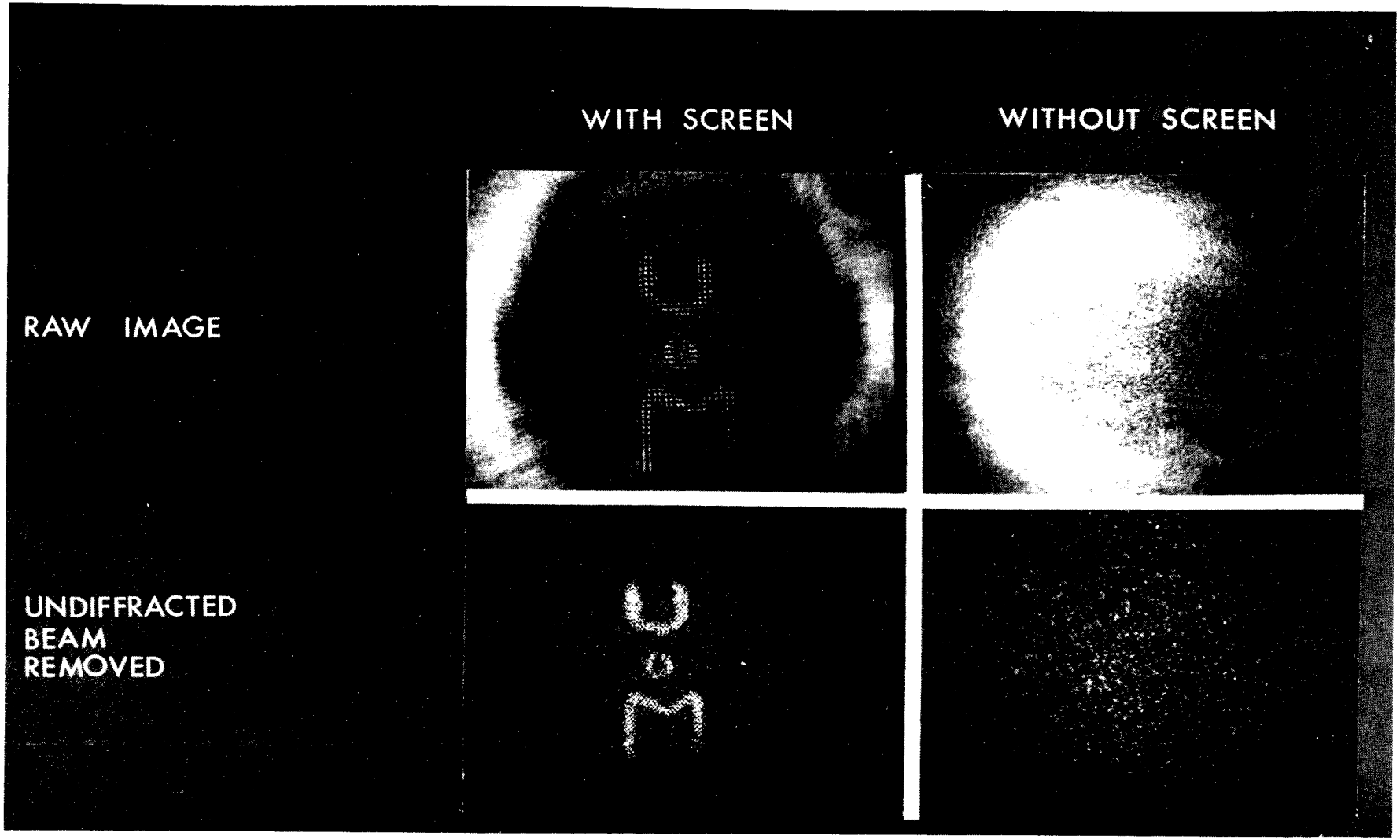
WITH SCREEN
WITHOUT SCREEN
RAW IMAGE
UNDIFFRACTED
BEAM
REMOVED

Figure 7.

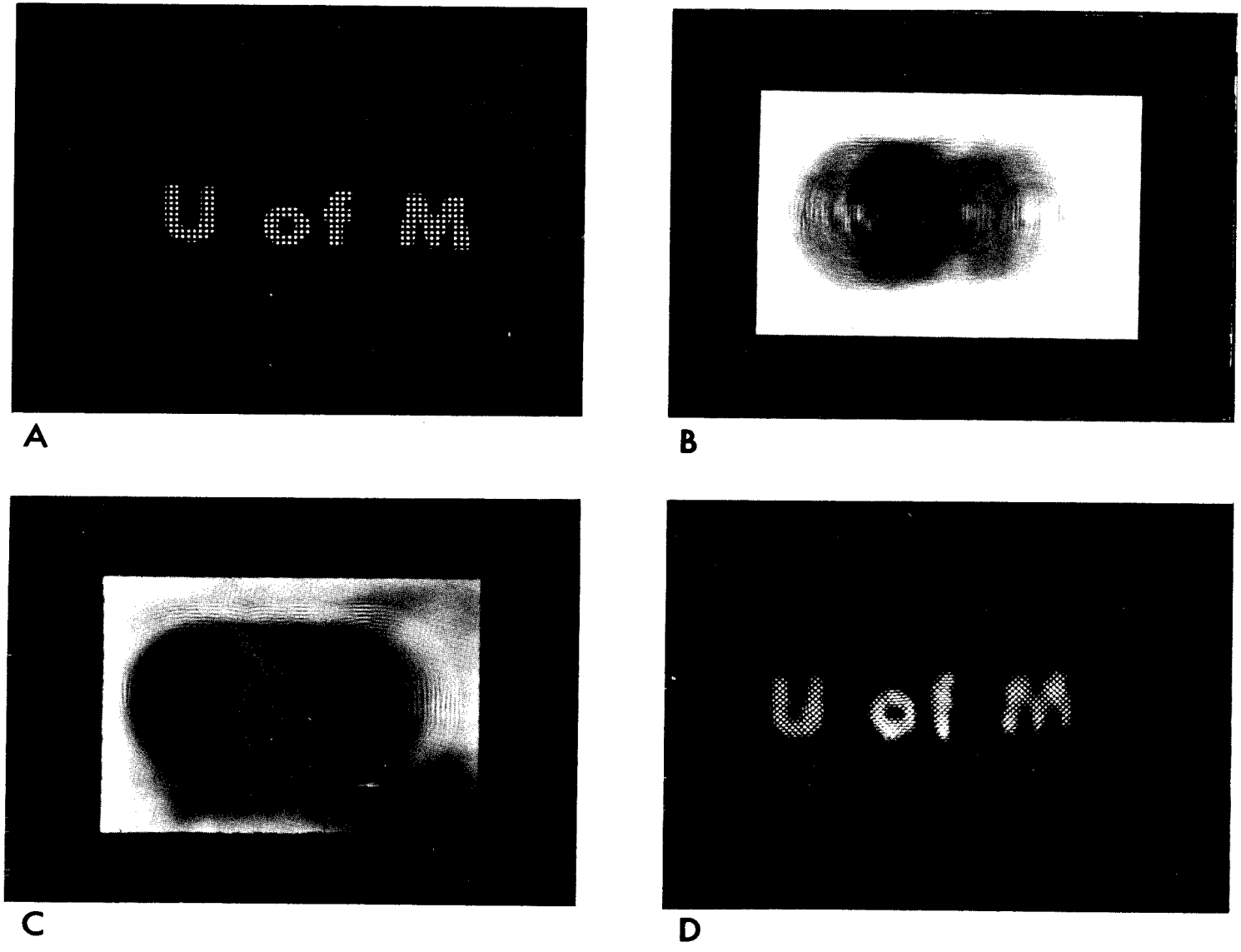

Figure 8.

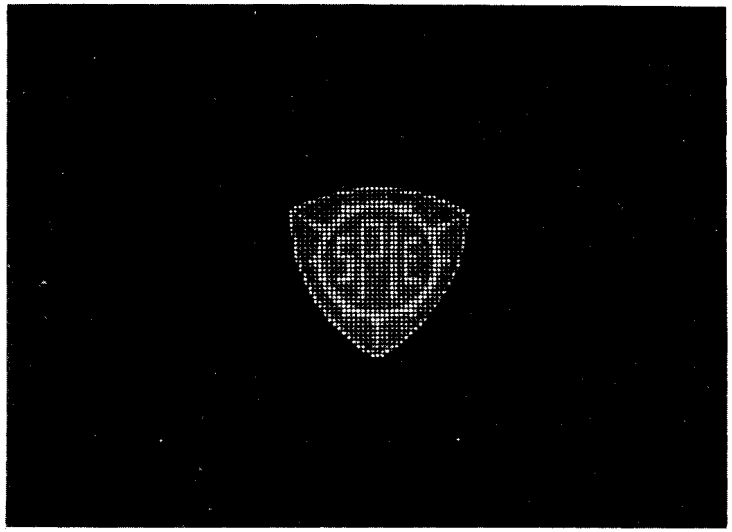

A

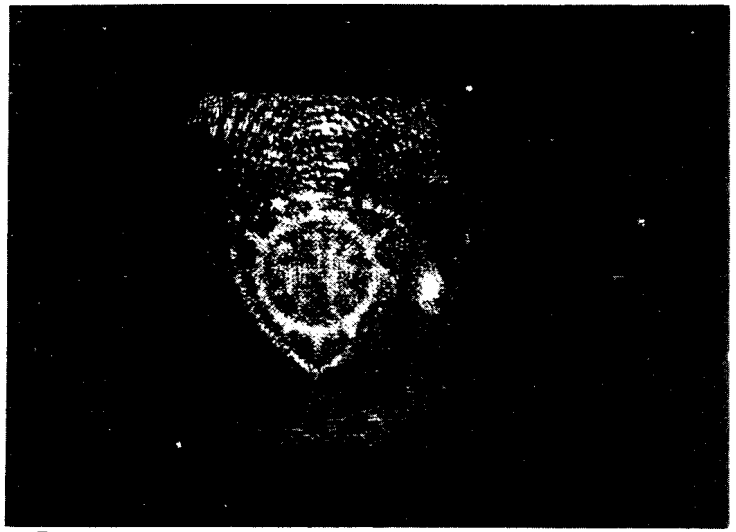

B

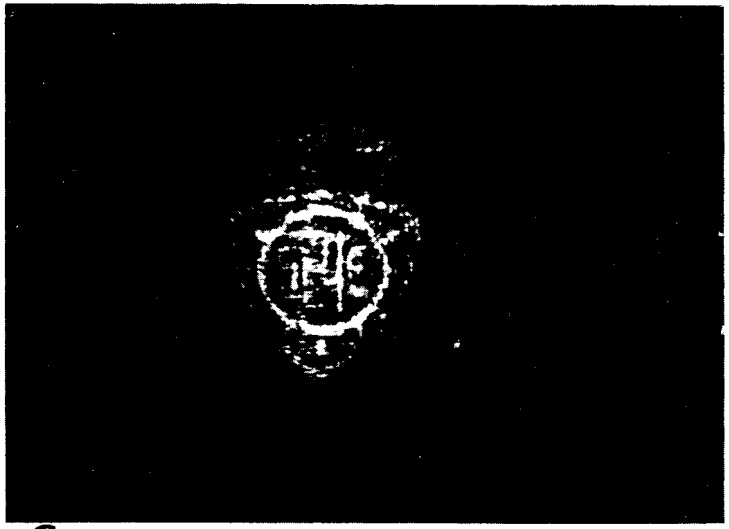

C

Figure 9..

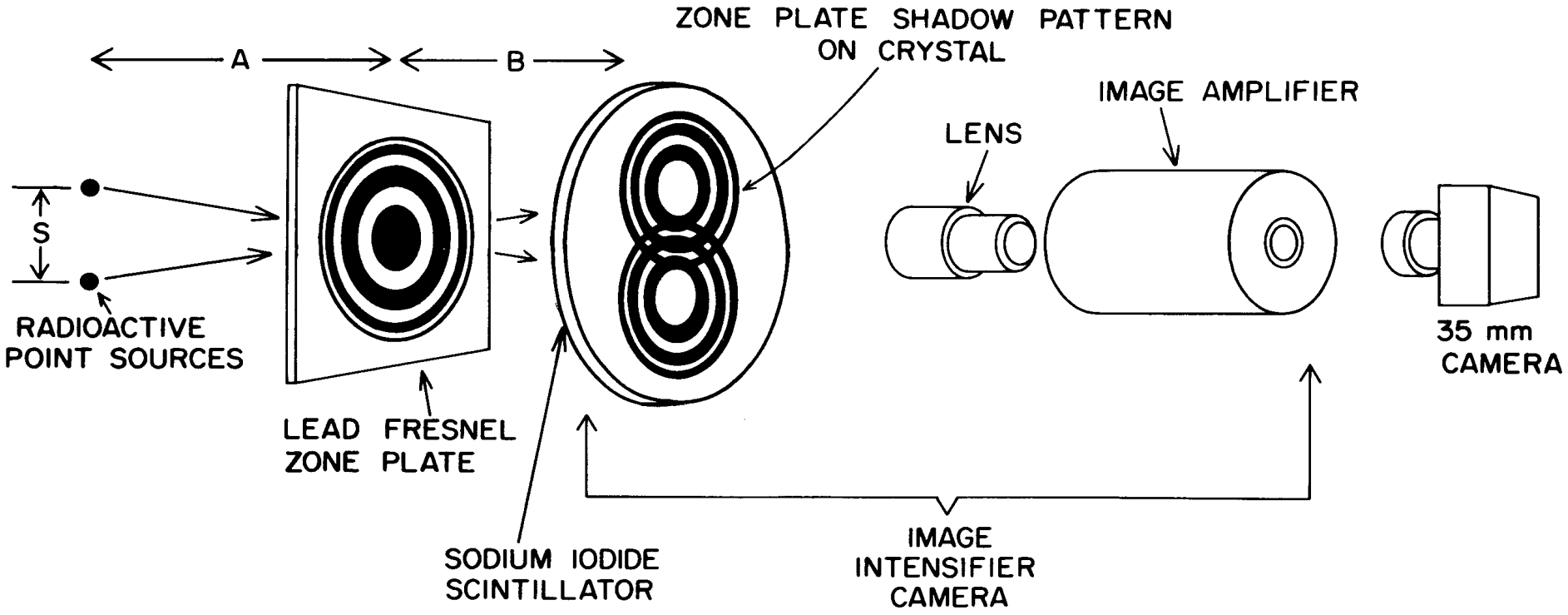
A
B
ZONE PLATE SHADOW PATTERN
ON CRYSTAL
IMAGE AMPLIFIER
LENS
S
RADIOACTIVE
POINT SOURCES
LEAD FRESNEL
ZONE PLATE
35 mm
CAMERA
SODIUM IODIDE
SCINTILLATOR
IMAGE
INTENSIFIER
CAMERA

Figure 10.

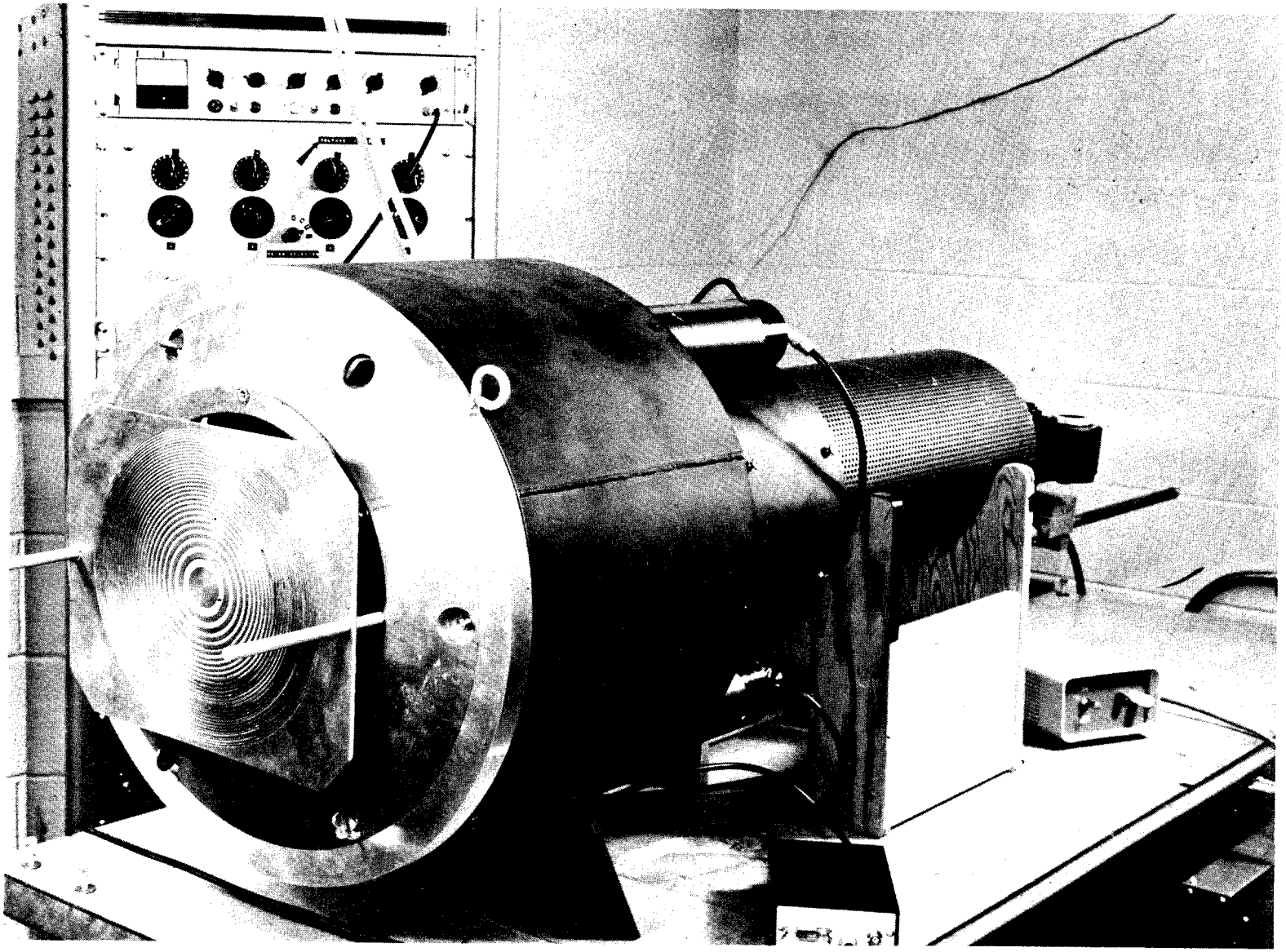

Figure 11.

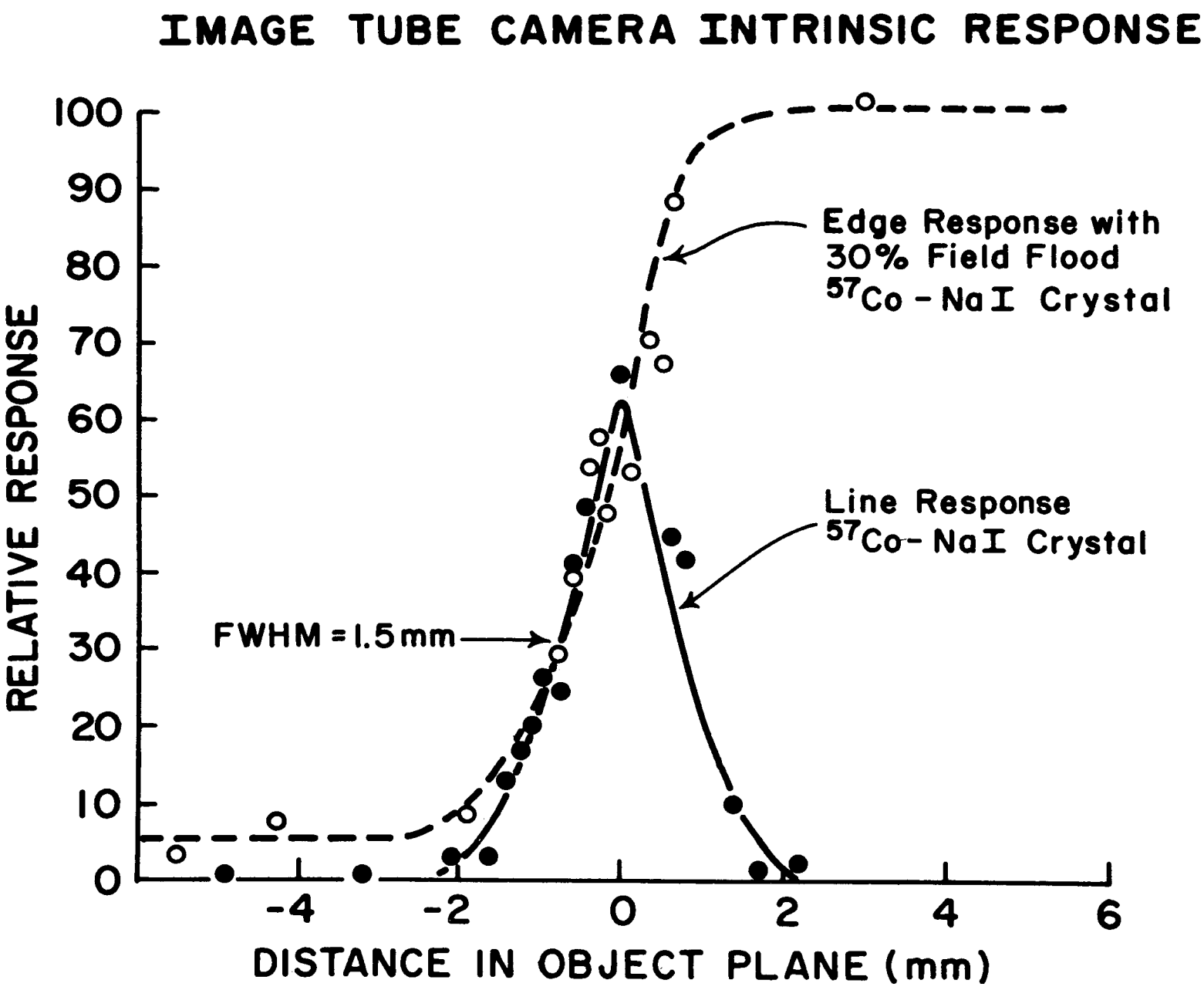
IMAGE TUBE CAMERA INTRINSIC RESPONSE
RELATIVE RESPONSE
100
90
80
70
60
50
40
30
20
10
0
-4
-2
0
2
4
6
DISTANCE IN OBJECT PLANE (mm)
Edge Response with
30% Field Flood
57Co - NaI Crystal
Line Response
57Co - NaI Crystal
FWHM = 1.5mm

Figure 12.

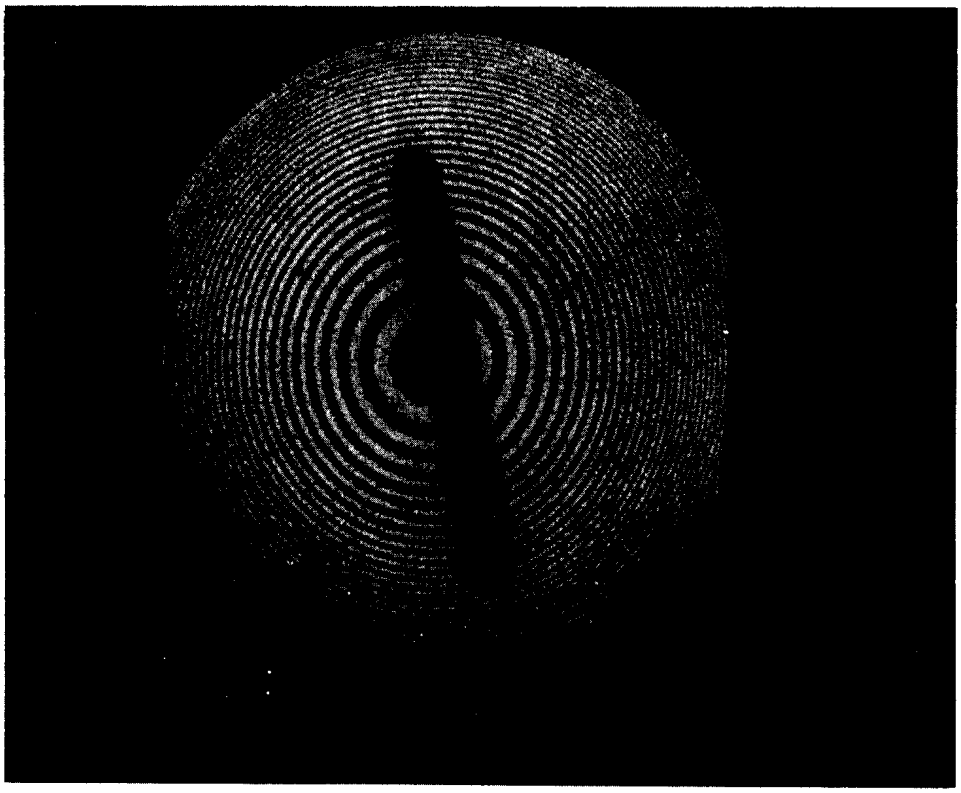

A

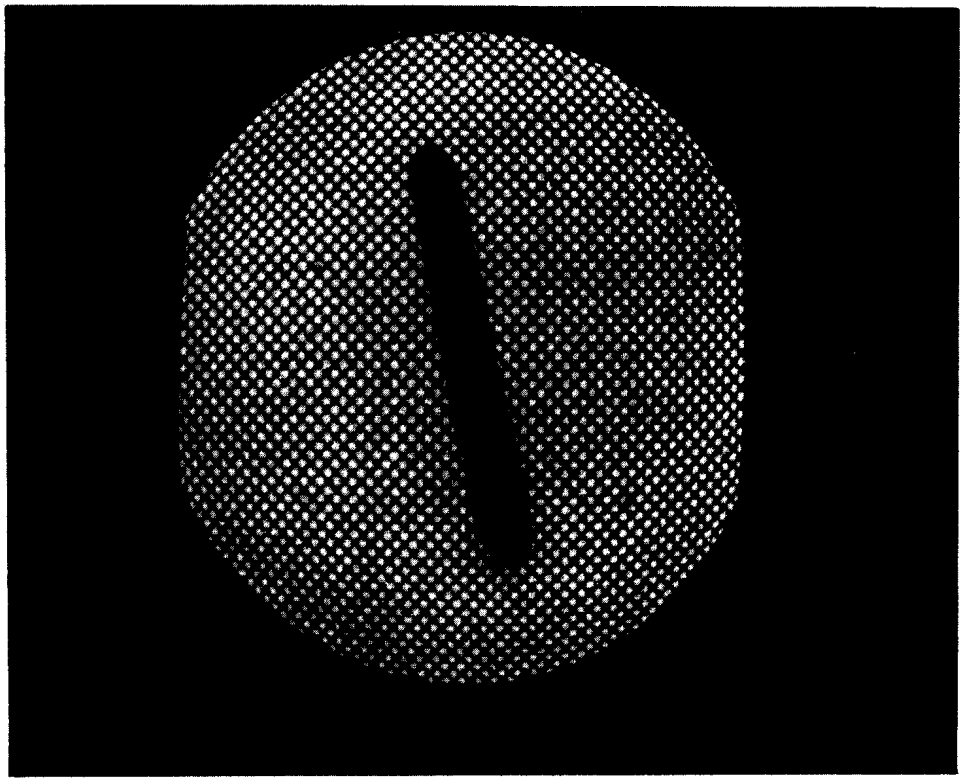

B

Figure 13.

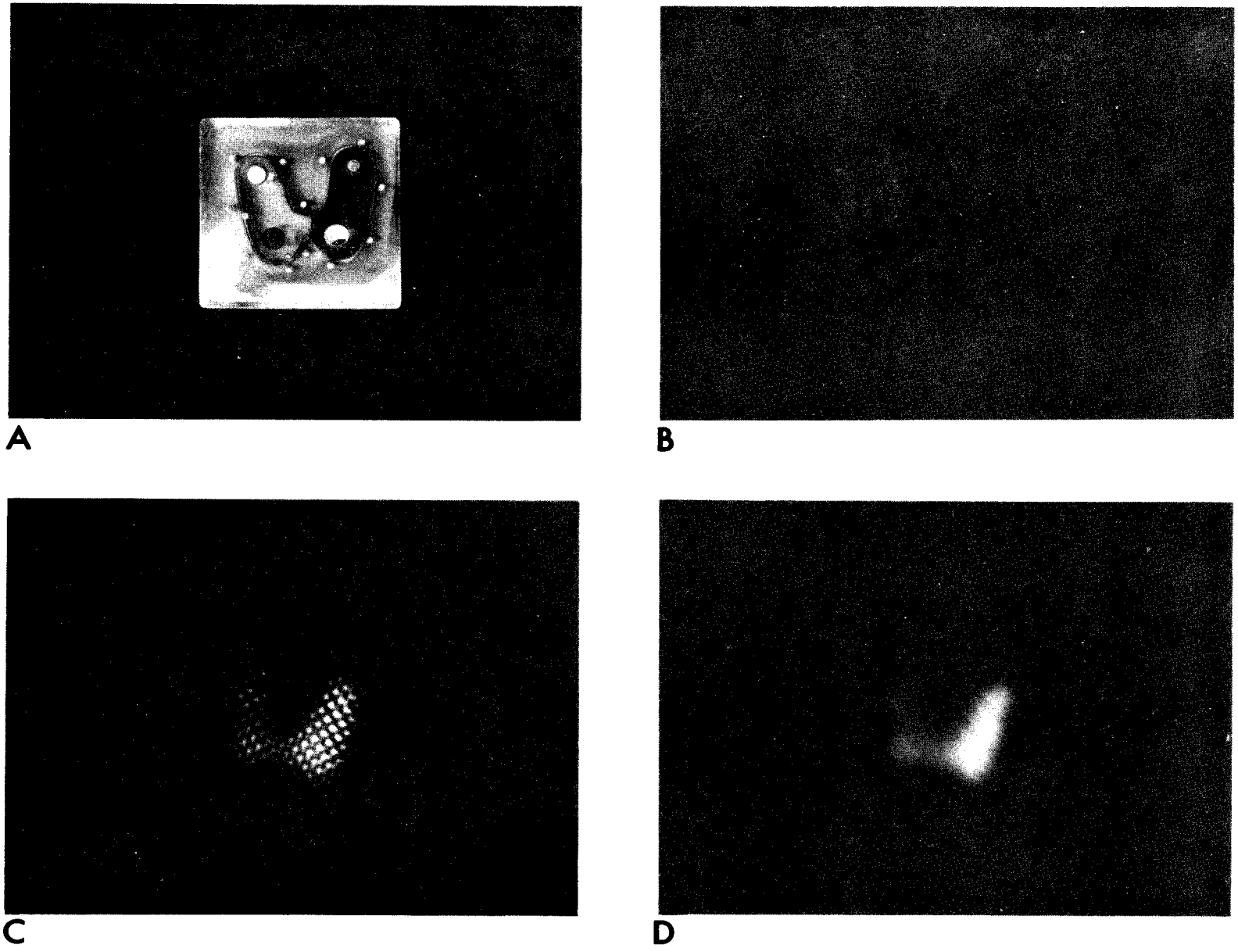

Figure 14.

References

1. Mertz, L., Young, N.O.: "Fresnel Transformation of Images." In Proc. Int. Conf. Optical Inst., London (1961) p. 305.
2. Barrett, H.H.: "Fresnel Zone Plate Imaging in Nuclear Medicine." Journal of Nuclear Medicine 13, 382 (1972).
3. Dicke, R.H.: " Scatter-hole Cameras for X-rays and Gamma-rays." Astrophysical J. 153, L 101 (1968).
4. Hayat, G.S.: "X-ray and γ-ray Imaging with Multiple Pin-hole Cameras." Ph.D. Thesis, State University of New York at Stony Brook; (1971), University Microfilm #72-9848.
5. Stigliani, D.J., Mittra, R., Semonin, R.G.: "Resolving Power of a Zone Plate," J.O.S.A. 57, 610 (1967).
6. Rogers, W.L., Han, K.S., Jones, L.W., Beierwaltes, W.H.: "Application of a Fresnel Zone Plate to Gamma-ray Imaging," Journal of Nuclear Medicine 13, 612 (1972).
7. Rogers, W.L., Han, K.S., Jones, L.W., Beierwaltes, W.H.: "Use of Incoherent Holography for Gamma-ray Imaging," Abs. Journal of Nuclear Medicine 13, 464 (1972).
8. Goodman, J.W.: "Film-Grain Noise in Wavefront Reconstruction Imaging," J.O.S.A. 57, 493 (1967).
9. Kosma, A.: "Effects of Film-Grain Noise in Holography," J.O.S.A. 58, 436 (1968).
10. Kosma, A.: "Incoherent Holography," presented at 1968 Spring Meeting, Optical Society of America, 14 March, 1968.
11. Barrett, H.H., Wilson, D.T. and DeMeester, G.D.: " The Use of Half-Tone Screens in Fresnel Zone Plate Imaging of Incoherent

Sources," Opt. Comm. 5, 398 (1972).

12. Rogers, W.L., Thomas, F.D., Beierwaltes, W.H., Colvin, T.: "The U.M.-Bendix Scintillation Camera." Biomed. Sci. Instrum. 6, 248-255 (1969)

13. Thomas, F.D., Beierwaltes, W.H., Knoll, G.F., Jones, L.W., Colvin, T., and Colestock, H.E.: "A New Scintillation Camera," International Atomic Energy Agency, Symposium on Medical Radioisotope Scintigraphy, Salzburg, Austria, August 6-15, 1968), pp 43-56.